Electrochimica Acta 108 (2013) 827–832

Contents lists available at ScienceDirect

Electrochimica Acta

journal homepage: www.elsevier.com/locate/electacta

Synthesis of $LiNi_xFe_{1-x}PO_4$ solid solution as cathode materials for lithium ion batteries

Rui Qing[a,1], Ming-Che Yang[b], Ying Shirley Meng[b], Wolfgang Sigmund[a,*]

[a] Department of Materials Science and Engineering, University of Florida, USA
[b] Department of NanoEngineering, UC San Diego, USA

ARTICLE INFO

Article history:
Received 26 February 2013
Received in revised form 3 July 2013
Accepted 3 July 2013
Available online 16 July 2013

Keywords:
$LiNiPO_4$
$LiFePO_4$
Lithium ion battery
Solid solution
Chemical delithiation

ABSTRACT

Nanosize $LiNi_xFe_{1-x}PO_4$ solid solution and $LiNi_xFe_{1-x}PO_4$/C nanocomposites were prepared via a solid state reaction method under argon atmosphere. A single phase olivine-type structure with Pnma space group was determined by X-ray diffraction. Crystallite sizes were found to be around 50 nm. A linear relationship was observed between lattice parameters and chemical composition which follows Vegard's law. Synthesized materials displayed electronic conductivity similar to previous reported values of $LiFePO_4$. Carbon coating further increased the overall conductivity of nanocomposites to the order of 10^{-3} S/cm. Chemical delithiation via NO_2BF_4 oxidant extracted more than 95% of lithium from the solid solution material accompanied by a decrease in lattice parameters.

1. Introduction

Since the discovery of the electrochemical reactivity of $LiFePO_4$ [1], olivine structure materials have been under investigation as cathodes for lithium ion batteries, especially with focus toward electric vehicle (EV) and plug-in hybrid vehicle (PHV) applications [2–4]. One dimensional lithium transport channels are observed along the [0 1 0] direction [5,6]. Olivine type structures are of interest as cathode materials in lithium ion batteries due to their abundance in nature, low cost, reduced toxicity and good electrochemical performance [7,8]. A near theoretical reversible capacity between 160 and 170 mAh/g has already been achieved in $LiMnPO_4$ and $LiFePO_4$ [9,10]. Among the four types of lithium transition metal phosphates, $LiNiPO_4$ has the highest operation voltage of 5.1 V against lithium metal, according to computational results [11–13,8]. The value is significantly superior to the currently commercialized $LiFePO_4$ which has an operation voltage around 3.4 V. However, it was hypothesized that the $\sim 10^{-14}$ S/cm intrinsic electronic conductivity of $LiNiPO_4$ based materials, which is 4–5 orders lower than the conductivity for $LiFePO_4$ (10^{-7} to 10^{-9} S/cm), prevents activation of the Ni^{2+}/Ni^{3+} redox pair. Therefore no one before has achieved any observable electrochemical reactivity for this cathode material [14–17].

Due to the common poor intrinsic conductivity of olivine type materials, several approaches were developed to improve their electrical performance. The most widely used method is the minimization of particle size, which decreased the electron conductor length and increased their specific surface area as well as the ternary interface of the electron conductor with the electrolyte [18,19]. The electron conductor properties can also be improved by application of a thin carbon coating on the lithium transition metal phosphates. Nanosize particles further enhance the charge/discharge process by reducing the overall ion solid diffusion length for the lithium ions. [9,20]. By combining the reduction of particle size and forming $LiFePO_4$/C composites, materials with near theoretical electrochemical capacity had been obtained. Additionally, Y.M. Chiang et al. proposed that aliovalent ion doping on lithium sites within the lattice would promote the intrinsic electronic conductivity of $LiFePO_4$ by an order of 8, but the overall feasibility and effectiveness of this aliovalent doping approach are still under debate [21–26].

Beyond the above mentioned approaches the overall electronic conductivity as well as electrochemical performance of any olivine type materials can be enhanced via solid solutions. This involves the formation of a solid solution on the transition metal (M2) sites in the lattice (e.g.: Fe/Mn, Fe/Ni, Co/Ni, etc.) [6,14,16,27–29]. By substituting M2 site transition metal with another metal ion, it was expected

* Corresponding author at: Department of Materials Science and Engineering, University of Florida, 225 Rhines Hall, 32611, USA; WCU Department of Energy Engineering, Hanyang University, Seoul 133-791, Korea. Tel.: +1 352 846 3343; fax: +1 352 846 3355.
E-mail addresses: clarvioson@ufl.edu (R. Qing), wsigm@mse.ufl.edu (W. Sigmund).
[1] Department of Materials Science and Engineering, University of Florida, 235 Rhines Hall, 32611, USA.

0013-4686/$ – see front matter © 2013 Elsevier Ltd. All rights reserved.
http://dx.doi.org/10.1016/j.electacta.2013.07.032

that the conductivity of the low end member could be increased by the introduction of higher conductivity counterparts. Consequently the overall electrochemical performance could be enhanced.

The solid solution between $LiFePO_4$ and $LiNiPO_4$ had previously been of interest mainly because of the enhancement of $LiFePO_4$'s cycling and rate performance by introducing nickel content into their lattice [27,28]. Efforts were mostly made in Fe-rich region of the binary system (nickel content <0.1). To date no publication had reported the synthesis and structural properties of the $LiFePO_4$–$LiNiPO_4$ solid solution system with high nickel content, which would be crucial for the electrochemical activity on Ni^{2+}/Ni^{3+} redox couple to be realized.

In this paper, we reported the synthesis and structural properties of the whole series of $LiNi_xFe_{1-x}PO_4$ solid solution material ($x = 0, 0.2, 0.4, 0.6, 0.8, 1$). These solid solutions as well as pure materials were synthesized with and without the additive of cellulose, which served as source for surface carbon coating. The difference in their electronic conductivity was characterized by 4 point probe test. Phase purity for these two series of solid solutions was confirmed by X-ray diffraction whereas crystallite sizes and lattice parameters were also calculated. Morphology of the materials was examined by field-emission scanning electron microscopy. Chemical delithiation was used to determine the lithium content that was able to be removed from the solid solution lattice and compared with electrochemically charged material (cycled to 4.3 V). Corresponding X-ray diffraction was conducted to examine the change in lattice with the removal of lithium content. This is the first article where the synthesis of phase pure $LiNi_xFe_{1-x}PO_4$ solid solution nano-materials was reported. Also for the first time the delithiation with 90% is reported.

2. Experimental

2.1. Synthesis

$LiNi_xFe_{1-x}PO_4$ solid solution nanocomposites were prepared via solid state reaction method. Li_2CO_3 (lithium carbonate, 99.5+%, A.C.S certified, Fisher Scientific), FeC_2O_4 (iron (ii) oxalate dihydrate, 99+%, Alfa Aesar), $Ni(CH_3COO)_2$ (nickel(ii) acetate tetrahydrate, 99+%, for analysis, Acros organics) and $NH_4H_2PO_4$ (ammonium dihydrogen phosphate, 99+%, for analysis, Acros organics) were used as raw material for synthesis. Cellulose (microcrystalline, Acros organics) was added to the solution for carbon coated nanocomposites. Stoichiometric amount of precursor materials were fully mixed by ball milling in acetone with zirconia media for 24 h. The mixture was then ground with pestle and mortar and dried in air at 80 °C, followed by heat treatment at 350 °C for 8 h in flowing argon for precursor decomposition. The calcined powders were then ground and pressed into pellets in air before final firing and crystallization at 650 °C for 10 h in argon. Different from the solid solution materials, pure phase $LiFePO_4$ was synthesized by the same heat treatment route but with cellulose additive and a vacuum system for stricter atmosphere control. $LiNiPO_4$ powders were obtained through a sol–gel route developed by Gaugulibabu et al. [30]. A few experiments were also done in nitrogen atmosphere and no observable difference between samples calcined in various atmospheres was detected.

2.2. Analysis

Surface morphology of the nanocomposites was characterized by FEI XL-40 field emission scanning electron microscopy. Samples were coated with a thin layer of Au–Pd. The crystal phases of the synthesized series of materials were determined by Philips APD 3720 X-ray diffractometer with CuKα source (λ = 1.54178 Å). The diffraction pattern was collected through a 2θ angle from 10° to 80° at a speed of 0.04° per second. A collinear 4 point probe setup was used to measure the electronic conductivity of disk-shaped fired samples. Pellets used for the characterization were 1 cm in diameter and 1 mm in thickness. Samples were polished before the test to provide uniform surfaces for contacts.

In order to evaluate the capability for insertion/removal of lithium in those nanocomposites, chemical delithiation experiments with strong oxidant NO_2BF_4 were conducted. The reaction goes as follows:

$$LiNi_xFe_{1-x}PO_4 + NO_2BF_4 \rightarrow Li_{1-y}Ni_xFe_{1-x}PO_4 + yNO_2 + yLiBF_4 + (1-y)NO_2BF_4$$

NO_2BF_4 oxidant was dissolved in 99% anhydrous acetonitrile (Acros Organics) before reaction. Selected composition of synthesized material was then mixed with the solution in atomic ratio 1:1 and 1:2 against NO_2BF_4. After delithiation, the material was washed with acetonitrile repeatedly and left drying for 24 h. The whole process was done in an argon filled glove box with strict atmospheric controls to prevent any potential oxidation of the reactants. Finally the dry powder was characterized by X-ray diffraction for pattern analysis. For comparison purposes, electrochemically charged cathode materials with the same composition was also analyzed. Due to the limitation of the electrolyte used ($LiPF_6$ in ethylene carbonate: dimethyl carbonate), only low voltage electrochemical cycles up to 4.3 V were able to be conducted. Three charging processes and two discharging processes were applied to the cathode in a CR2016 coin cell setup at a C rate of C/20. Lithium metal was used as the counter-electrode with Celgard 260 as separator. Assembly and disassembly of the coin cells were always done in argon atmosphere in the glove box. Upon completion of electrochemical cycles the coin cell was taken apart; the cathode material was washed with acetonitrile (99%, anhydrous) and dried overnight before taking out for XRD analysis. The diffraction pattern was then refined with FullProf Suite version 1.10, 2009 by the Institute Laue-Langevin, Grenoble, France to obtain crystallography information.

3. Results and discussion

3.1. Synthesis and characterization

The morphology for the solid solution materials is shown in Fig. 1. Primary particles with diameters in the range from 40 nm to 200 nm are found. Small particles are seen to adhere to larger particles of microns to several microns. These larger particles of several microns are most likely aggregates or agglomerates of primary crystals according to the X-ray data analysis which will follow. For carbon coated nanocomposites (not shown in the figure) the particles appeared highly connected due to the embedding in the carbon matrix.

Fig. 2 shows the X-ray diffraction patterns for $LiNi_xFe_{1-x}PO_4$ ($x = 0, 0.2, 0.4, 0.6, 0.8, 1$) series solid solution materials synthesized without carbon coating. It was found that all peaks could be indexed to a single phase of ordered olivine type structure belonging to orthorhombic Pnma space group. No peaks related to alternative phases had been detected in the graph. Thus it was concluded that high phase purity series of $LiNi_xFe_{1-x}PO_4$ solid solution materials were synthesized with the solid state reaction routes described above. Similar to the pure $LiFePO_4$ or $LiNiPO_4$ material, in the solid solution transition metal ion still occupied the octahedral M2 site homogeneously in a ratio determined by the precursor materials. All diffraction peaks are sharp and distinguishable that no obvious phase separation could be found. All synthesized samples displayed a grayish color similar to the color of carbon-free $LiFePO_4$ material as described in literature.

In Fig. 3, selected X-ray diffraction patterns were presented for $LiNi_xFe_{1-x}PO_4$ series solid solution materials synthesized with

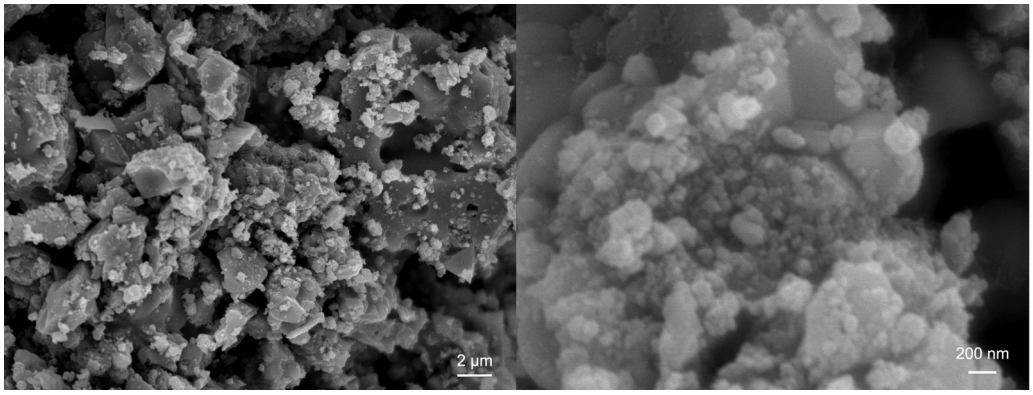

Fig. 1. Field-emission scanning electron microscopy picture for $LiNi_{0.6}Fe_{0.4}PO_4$ (selected) nanocomposites without carbon coating in low and high magnifications.

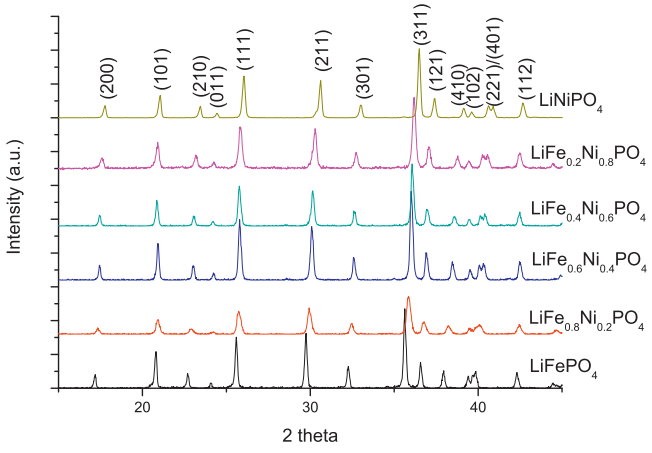

Fig. 2. X-ray diffraction patterns for $LiNi_xFe_{1-x}PO_4$ solid solution nanocomposites without carbon coating.

surface carbon coating. Alternative phases evolved during the synthesis process, marked with a star label in the graph. The phases were labeled to be nickel phosphides such as Ni_3P, Ni_7P_3, etc. These phases were believed to emerge from the reducing atmosphere created by the excessive carbon content from decomposition of the cellulose. Most likely the nickel ions were subjected to transition from $[Ni^{3+}]$ to $[Ni^{2+}]$ state in reducing atmosphere, through which these off-stoichiometric impurity phases were formed. These impurity phases would decrease the overall electrochemical capacity, but were beneficial in overall electronic conductivity as proposed by Nazar et al. [31]. Superior charge–discharge capacity and cycleability were observed for our carbon-coated sample tested toward a low voltage limit at 4.5 V as compared to the non-carbon coated ones.

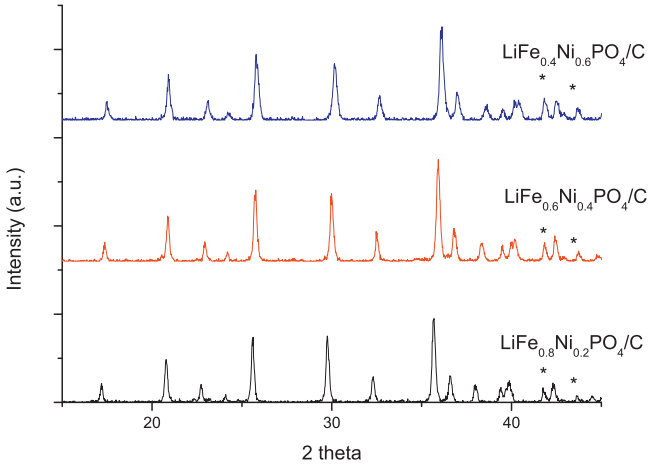

Fig. 3. X-ray diffraction patterns for $LiNi_xFe_{1-x}PO_4$ solid solution nanocomposites with carbon coating.

Based on the XRD graphs, lattice parameters for as-prepared nanocomposites were calculated using least square method and summarized in Table 1. The results were plotted against composition in Fig. 4, where *a*, *b*, *c* denoted the three dimensions of the orthorhombic cell. A linear correlation between lattice parameters and the content ratio of nickel in the composition was found. Lattice parameters *a* and *b* decreased linearly with the increasing ratio of nickel due to the smaller Shannon radii of $[Ni^{2+}]$ (0.69 Å) compared to $[Fe^{2+}]$ (0.78 Å). Lattice parameter *c* remained relatively unchanged. For the carbon coated $LiNi_xFe_{1-x}PO_4$ nanocomposites, lattice parameters *a* and *b* were slightly larger than that of carbon-free sample with the same composition. This could correspond to the fact that off-stoichiometric impurity phases of nickel phosphide (Ni_3P, Ni_7P_3) were formed due to the reducing atmosphere. Some of the nickel content may be partially consumed so the main phase switches toward the iron rich end. Selected samples had also been chosen to do multiple XRD tests in order to establish an error bar for the calculation. With repeated experiments the standard deviation for this test was determined to be ±0.5%.

Crystallite sizes for these nanocomposites were calculated by the Scherrer equation:

$$\tau = \frac{K\lambda}{\beta \cos\theta}$$

where *K* is the shape factor of 0.9 for spherical crystals, λ is the X-ray wavelength, β is half maximum intensity broadening (FWHM) in radians corrected for the instruments standard line width, and θ is the Bragg angle. τ is the calculated mean size of the crystalline domains, equal to the particle size of single crystallites. Crystal lengths along the three strongest peaks were calculated. No dendritic growth was observed. Typical crystallite size of 42 ± 9 nm for

Table 1
Lattice parameter for $LiNi_xFe_{1-x}PO_4$ solid solution materials.

Composition	*a* (Å)	*b* (Å)	*c* (Å)
$LiFePO_4$	10.328	6.003	4.692
$LiNi_{0.2}Fe_{0.8}PO_4$	10.240	5.964	4.662
$LiNi_{0.4}Fe_{0.6}PO_4$	10.178	5.922	4.663
$LiNi_{0.6}Fe_{0.4}PO_4$	10.149	5.877	4.682
$LiNi_{0.8}Fe_{0.2}PO_4$	10.096	5.846	4.676
$LiNiPO_4$	10.060	5.776	4.683
$LiNi_{0.2}Fe_{0.8}PO_4/C$	10.308	5.961	4.693
$LiNi_{0.4}Fe_{0.6}PO_4/C$	10.213	5.891	4.663
$LiNi_{0.6}Fe_{0.4}PO_4/C$	10.154	5.869	4.681

Table 2
Lattice parameters in Ångstrom and lithium occupancy for charged and chemically delithiated $LiNi_{0.6}Fe_{0.4}PO_4$ solid solution materials.

Sample\Parameter	*a* (Å)	*b* (Å)	*c* (Å)	Li^+ occupancy
$LiNi_{0.6}Fe_{0.4}PO_4$ sample	10.152	5.917	4.676	1.00
$LiNi_{0.6}Fe_{0.4}PO_4$ 2.5 cycle charged sample	10.026	5.865	4.667	0.59
$LiNi_{0.6}Fe_{0.4}PO_4$ 1:1 NO_2BF_4 24 h delithiation	9.931	5.817	4.704	0.23
$LiNi_{0.6}Fe_{0.4}PO_4$ 1:2 NO_2BF_4 24 h delithiation	9.908	5.806	4.703	0.05

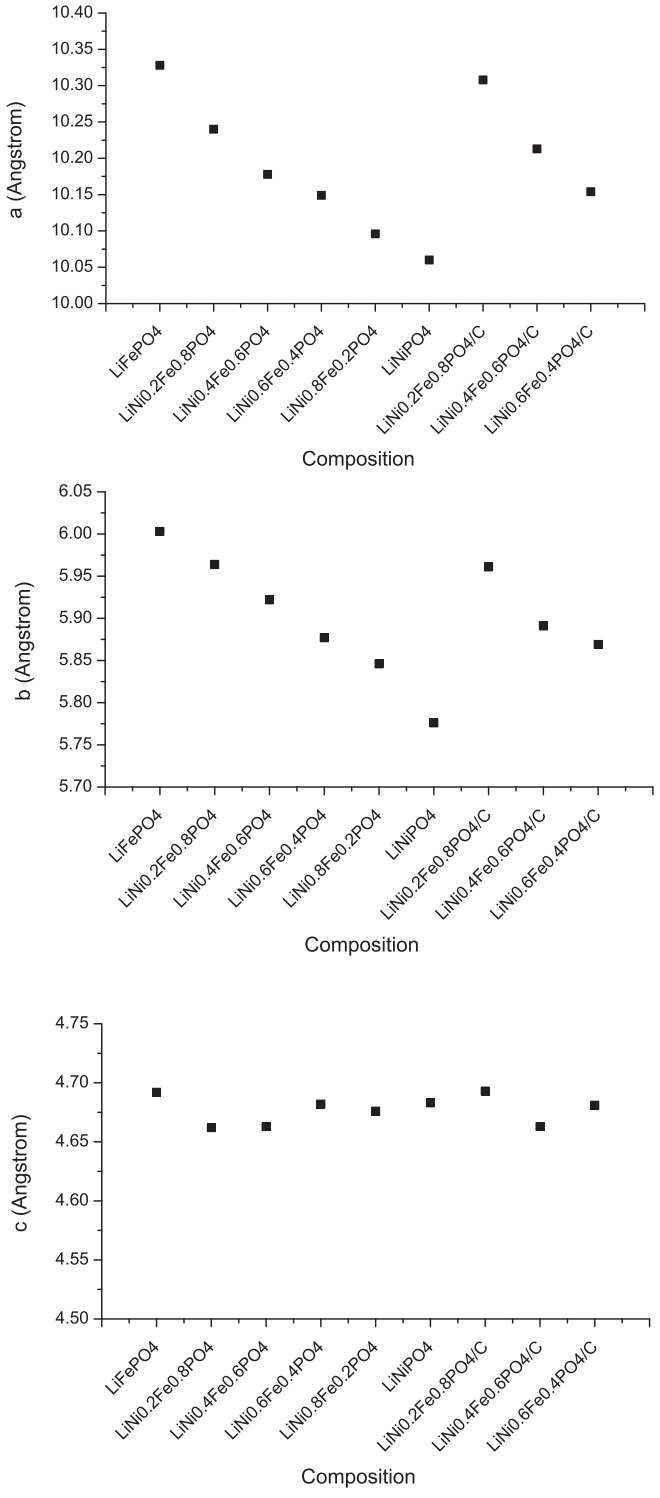

Fig. 4. Lattice parameter for $LiNi_xFe_{1-x}PO_4$ and $LiNi_xFe_{1-x}PO_4$/C nanocomposites follow Vegard's law.

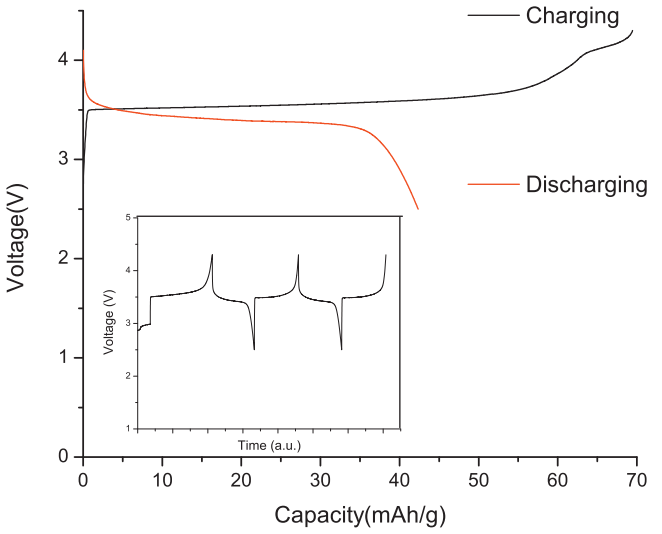

Fig. 5. Charging/discharging profile for the comparison test of chemical delithiation of $LiNi_{0.6}Fe_{0.4}PO_4$ nanocomposites (insert shows the charge/discharge test with time (arbitrary units)).

as-prepared samples was obtained. No correlation between crystallite size and composition has been found for the solid solution compounds. Also no significant change in the crystallite size had been observed when introducing carbon coating into the solid solution system.

Solid solutions without carbon coating were found to have conductivities in the order of 10^{-7} to 10^{-9} S/cm, while increased iron content enhanced the conductivity 1–2 orders of magnitude compared to pure $LiNiPO_4$ by using 4 point probe. Conductivities for nanocomposites synthesized with carbon coatings were determined to be 10^{-2} to 10^{-3} S/cm. These conductivities show significant improvement in conductivity for these $LiNi_xFe_{1-x}PO_4$/C nanocomposites. They are attributed to a continuous phase of amorphous carbon content on the particle surface.

3.2. Chemical delithiation test

Fig. 6 shows the XRD diagrams for one type of nanocomposites, i.e. $LiN_{i0.6}Fe_{0.4}PO_4$ in its pure phase; electrochemically charged; chemically delithiated with NO_2BF_4 ratio 1:1; and chemically delithiated with NO_2BF_4 ratio 1:2. The electrochemical delithiation process and its first cycle charge–discharge capacity are shown in Fig. 5. Starting from the pure phase $LiN_{i0.6}Fe_{0.4}PO_4$ nanocomposite the peaks shift toward higher 2 theta angles which is shown in Fig. 5. The shift of the peaks correspond to the lattice planes indicating the contraction of the whole crystal lattice, which is induced by the removal of lithium from the oxygen octahedrons.

Using the least square method, single cell parameters for electrochemically charged and chemically delithiated $LiNi_{0.6}Fe_{0.4}PO_4$ nanocomposites with lithium partially removed were calculated and compared to the as-prepared sample. Significant contraction in lattice parameters *a* and *b* was found for both samples, while the change in lattice parameters for the chemically delithiated samples were much greater. This could be attributed to the

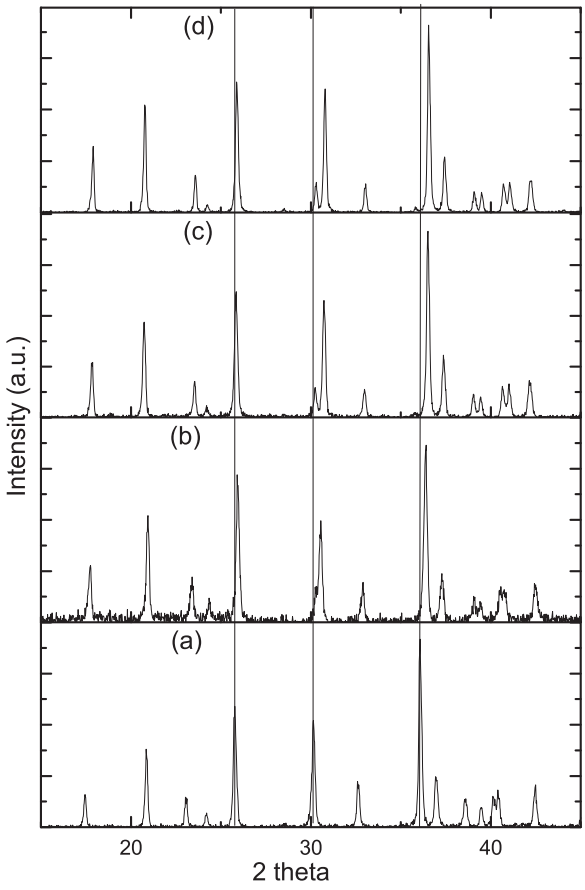

Fig. 6. X-ray diffraction pattern for (a) pure phase $LiNi_{0.6}Fe_{0.4}PO_4$ nanocomposites; (b) electrochemically charged $LiNi_{0.6}Fe_{0.4}PO_4$; (c) chemically delithiated $LiNi_{0.6}Fe_{0.4}PO_4$ with NO_2BF_4 ratio 1:1; (d) chemically delithiated $LiNi_{0.6}Fe_{0.4}PO_4$ with NO_2BF_4 ratio 1:2.

corresponding Fe^{2+}/Fe^{3+} redox couple that at low voltage electrochemical cycles up to 4.3 V limits delithiation, while the strong oxidant NO_2BF_4 was capable of also activating the Ni^{2+}/Ni^{3+} redox couple so more lithium could be extracted. Applying Rietveld refinement method using the FullProf Suite software, the lithium occupancy for the chemically delithiated samples was calculated and shown in Table 2. Related information is available in the supplementary material section. It was found that more than 95% of lithium content could be extracted from the crystal lattice with a chemical ratio of 1:2 for $LiNi_{0.6}Fe_{0.4}PO_4$ to NO_2BF_4, while NO_2BF_4 to $LiNi_{0.6}Fe_{0.4}PO_4$ at ration 1:1 could only remove 77% of lithium. These values far exceed the theoretical value of lithium content (40%) corresponding to the Fe^{2+}/Fe^{3+} redox couple alone and is evidence for the activation of Ni^{2+}/Ni^{3+} redox couple in the crystal lattice.

Based on the characterization data, it was concluded that two contributions from the iron substitution on nickel sites helped the activation of Ni^{2+}/Ni^{3+} redox couple in the solid solution material. The first enhancement was the increase in overall electronic conductivity whereas the electrons could be removed/added more freely for redox reactions, as presented in the 4 point probe tests. The second factor was not as straightforward as the first one. The introduction of iron actually slightly decreased the redox voltage, through which the reactions on the higher voltage end could become more tolerable to electrolytes, or as presented in this manuscript, to NO_2BF_4 oxidant. The decrease in voltage would be less than 0.5 V depending on actual composition, so it did not diminish the targeted voltage superior from $LiNiPO_4$ based material.

Having confirmed the reactivity of nickel content in our as-prepared $LiNi_xFe_{1-x}PO_4$ solid solution materials, further electrochemical tests with high voltage electrolyte would be needed to demonstrate the full potential of these series of materials as cathodes for lithium ion batteries. Testing of various high voltage electrolytes in combination with our $LiNi_xFe_{1-x}PO_4$ nanocomposites are ongoing and the results will be reported in the future.

4. Conclusions

A solid state reaction route was presented through which, for the first time, whole series of phase-pure $LiNi_xFe_{1-x}PO_4$ olivine type solid solution materials were synthesized and characterized. The crystallite size for the as-prepared samples was 40–50 nm. The primary particles appear to be highly agglomerated and aggregated. Lattice parameters of the nanocomposites changed linearly with the content change of M2 site transition metal ion as was expected from Vegard's law. The synthesized solid solutions displayed similar electronic conductivity of $LiFePO_4$. The introduction of a carbon source during synthesis could increase the overall conductivity to as high as 10^{-2} S/cm. Using strong oxidant NO_2BF_4, we were able to activate the Ni^{2+}/Ni^{3+} redox couple and remove more than 95% of the total lithium content in the material, which proved the feasibility of using iron solid solution to activate the $LiNiPO_4$ based material.

Acknowledgment

One of the authors (W.S.) acknowledges support by WCU (World Class University) program through the National Research Foundation of Korea funded by the Ministry of Education, Science and Technology (R31-100092).

Appendix A. Supplementary data

Supplementary data associated with this article can be found, in the online version, at http://dx.doi.org/10.1016/j.electacta.2013.07.032.

References

[1] A.K. Padhi, K.S. Nanjundaswamy, J.B. Goodenough, Phospho-olivines as positive-electrode materials for rechargeable lithium batteries, Journal of the Electrochemical Society 144 (1997) 1188–1194.
[2] H. Huang, S.C. Yin, L.F. Nazar, Approaching theoretical capacity of $LiFePO_4$ at room temperature at high rates, Electrochemical and Solid State Letters 4 (2001) A170–A172.
[3] M.S. Whittingham, Lithium Batteries and Cathode Materials, Chemical Reviews (2004) 4271–4301.
[4] A. Yoshino, Development of lithium ion battery, Molecular Crystals and Liquid Crystals 340 (2000) 425–429.
[5] S. Okada, S. Sawa, M. Egashira, J. Yamaki, M. Tabuchi, H. Kageyama, T. Konishi, A. Yoshino, Cathode properties of phospho-olivine $LiMPO_4$ for lithium secondary batteries, Journal of Power Sources 97/8 (2001) 430–432.
[6] D. Shanmukaraj, R. Murugan, Synthesis and characterization of $LiNiyCo1\text{-}yPO_4$ (y = 0-1) cathode materials for lithium secondary batteries, Ionics 10 (2004) 88–92.
[7] Y.D. Cho, G.T.K. Fey, H.M. Kao, The effect of carbon coating thickness on the capacity of $LiFePO_4$/C composite cathodes, Journal of Power Sources 189 (2009) 256–262.
[8] C.A.J. Fisher, V.M.H. Prieto, M.S. Islam, Lithium battery materials $LiMPO_4$ (M = Mn, Fe, Co, and Ni): Insights into defect association, transport mechanisms, and doping behavior, Chemistry of Materials 20 (2008) 5907–5915.
[9] G.H. Li, H. Azuma, M. Tohda, $LiMnPO_4$ as the cathode for lithium batteries, Electrochemical and Solid State Letters 5 (2002) A135–A137.
[10] G.H. Li, H. Azuma, M. Tohda, Optimized $LiMnyFe1\text{-}yPO_4$ as the cathode for lithium batteries, Journal of the Electrochemical Society 149 (2002) A743–A747.
[11] Y.N. Xu, W.Y. Ching, Y.M. Chiang, Comparative studies of the electronic structure of $LiFePO_4$, $FePO_4$, $Li3PO_4$, $LiMnPO_4$, $LiCoPO_4$, and $LiNiPO_4$, Journal of Applied Physics 95 (2004) 6583–6585.

[12] O. Le Bacq, A. Pasturel, First-principles study of $LiMPO_4$ compounds (M = Mn, Fe, Co, Ni) as electrode material for lithium batteries, Philosophical Magazine 85 (2005) 1747–1754.
[13] W.F. Howard, R.M. Spotnitz, Theoretical evaluation of high-energy lithium metal phosphate cathode materials in Li-ion batteries, Journal of Power Sources 165 (2007) 887–891.
[14] J. Wolfenstine, J. Allen, $LiNiPO_4$-$LiCoPO_4$ solid solutions as cathodes, Journal of Power Sources 136 (2004) 150–153.
[15] J. Wolfenstine, J. Allen, Ni^{3+}/Ni^{2+} redox potential in $LiNiPO_4$, Journal of Power Sources 142 (2005) 389–390.
[16] K. Rissouli, K. Benkhouja, J.R. Ramos-Barrado, C. Julien, Electrical conductivity in lithium orthophosphates, Materials Science and Engineering B: Solid State Materials for Advanced Technology 98 (2003) 185–189.
[17] T. Muraliganth, A. Manthiram, Understanding the Shifts in the Redox Potentials of Olivine LiM(1-y)M(y)PO(4) (M = Fe, Mn, Co, and Mg) Solid Solution Cathodes, Journal of Physical Chemistry C 114 (2010) 15530–15540.
[18] C. Delacourt, P. Poizot, M. Morcrette, J.M. Tarascon, C. Masquelier, One-step low-temperature route for the preparation of electrochemically active $LiMnPO_4$ powders, Chemistry of Materials 16 (2004) 93–99.
[19] A. Yamada, S.C. Chung, K. Hinokuma, Optimized $LiFePO_4$ for lithium battery cathodes, Journal of the Electrochemical Society 148 (2001) A224–A229.
[20] N. Ravet, Y. Chouinard, J.F. Magnan, S. Besner, M. Gauthier, M. Armand, Electroactivity of natural and synthetic triphylite, Journal of Power Sources 97-8 (2001) 503–507.
[21] S.Y. Chung, J.T. Bloking, Y.M. Chiang, Electronically conductive phospho-olivines as lithium storage electrodes, Nature Materials 1 (2002) 123–128.
[22] P.S. Herle, B. Ellis, N. Coombs, L.F. Nazar, Nano-network electronic conduction in iron and nickel olivine phosphates, Nature Materials 3 (2004) 147–152.
[23] M. Wagemaker, B.L. Ellis, D. Luetzenkirchen-Hecht, F.M. Mulder, L.F. Nazar, Proof of Supervalent Doping in Olivine $LiFePO_4$, Chemistry of Materials 20 (2008) 6313–6315.
[24] N. Meethong, Y.H. Kao, S.A. Speakman, Y.M. Chiang, Aliovalent Substitutions in Olivine Lithium Iron Phosphate and Impact on Structure and Properties, Advanced Functional Materials 19 (2009) 1060–1070.
[25] Y.M. Chiang, N. Meethong, Y.H. Kao, Reply to Comment on "Aliovalent Substitutions in Olivine Lithium Iron Phosphate and Impact on Structure and Properties", Advanced Functional Materials 20 (2010) 189–191.
[26] B.L. Ellis, M. Wagemaker, F.M. Mulder, L.F. Nazar, Comment on "Aliovalent Substitutions in Olivine Lithium Iron Phosphate and Impact on Structure and Properties", Advanced Functional Materials 20 (2010) 186–188.
[27] D.Y. Wang, H. Li, S.Q. Shi, X.J. Huang, L.Q. Chen, Improving the rate performance of $LiFePO_4$ by Fe-site doping, Electrochimica Acta 50 (2005) 2955–2958.
[28] Y. Lu, J.C. Shi, Z.P. Guo, Q.S. Tong, W.J. Huang, B.Y. Li, Synthesis of $LiFe_1$-xNixPO_4/C composites and their electrochemical performance, Journal of Power Sources 194 (2009) 786–793.
[29] J. Marzec, W. Ojczyk, J. Molenda, Delithiation of olivine – structured LiFexMn$_1$-xPO_4 cathode materials. Mossbauer studies, Materials Science – Poland 24 (2006) 69–74.
[30] Gangulibabu, D. Bhuvaneswari, N. Kalaiselvi, N. Jayaprakash, P. Periasamy, CAM sol-gel synthesized LiMPO4 (M = Co, Ni) cathodes for rechargeable lithium batteries, Journal of Sol–Gel Science and Technology 49 (2009) 137–144.
[31] B. Ellis, P.S. Herle, Y.H. Rho, L.F. Nazar, R. Dunlap, L.K. Perry, D.H. Ryan, Nanostructured materials for lithium-ion batteries: Surface conductivity vs. bulk ion/electron transport, Faraday Discussions 134 (2007) 119–141.